J. Fluid Mech. (2006), *vol.* 550, *pp.* 391–412.
doi:10.1017/S0022112005008116 Printed in the United Kingdom

Computational study on the internal layer in a diffuser

By XIAOHUA WU, JÖRG SCHLÜTER, PARVIZ MOIN, HEINZ PITSCH, GIANLUCA IACCARINO AND FRANK HAM

Center for Turbulence Research, Stanford University, CA 94305-3035, USA

(Received 18 November 2004 and in revised form 22 August 2005)

We report an internal layer found in the turbulent flow through an asymmetric planar diffuser using large-eddy simulation; we discuss five issues relevant to the internal layer: definition and identification, conditions for occurrence, connection with its outer flow, similarity with other equilibrium flows, and growth. The present internal layer exists in a region with stabilized positive skin friction downstream of a sharp reduction. The streamwise pressure gradient changes suddenly from slightly favourable to strongly adverse at the diffuser throat, and relaxes in a prolonged mildly adverse region corresponding to the skin friction plateau. Development of the internal layer into the outer region is slow, in contrast to the internal layers previously identified from certain external boundary-layer flows where the sudden change in streamwise pressure gradient is from strongly adverse to mildly favourable. Signatures of the internal layer include an inflectional point in the wall-normal profiles of streamwise turbulence intensity, and a well-defined logarithmic slope in the mean streamwise velocity underneath a linear distribution extending to the core region of the diffuser. Some of these characteristics bear a certain resemblance to those existing in the C-type of Couette–Poiseuille turbulent flows. Frequency spectrum results indicate that application of strong adverse pressure gradient at the diffuser throat enhances the low-frequency content of streamwise turbulent fluctuations. Inside the internal layer, the frequency energy spectra at different streamwise locations, but with the same wall-normal coordinate, nearly collapse. Two-point correlations with streamwise, wall-normal and temporal separations were used to examine connections between fluctuations inside the internal layer and those in the core region of the diffuser where the mean streamwise velocity varies linearly with distance from the wall. Galilean decomposition of instantaneous velocity vectors reveals a string of well-defined spanwise vortices outside the internal layer. The internal layer discovered from this study provides qualified support for a conjecture advanced by Azad & Kassab some years ago (*Phys. Fluids* A, vol. 1, 1989, p. 564).

1. Introduction

Identifying regions of self-preservation in representative non-equilibrium flows is useful for basic fluid mechanics as well as engineering computation. Townsend (1965, 1976) discussed the process that sudden changes in external conditions in boundary layers may result in an internal boundary layer that spreads from the section of change, and the layer outside the internal layer develops in almost the same way as in the original flow. Experimental evidence in support of this postulation includes

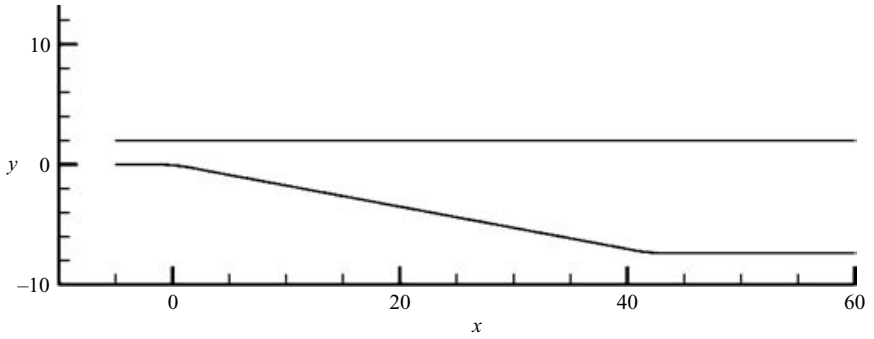

FIGURE 1. Cross-section of the asymmetric planar diffuser, the exit is at $x = 100$.

the boundary layer over a curved hill (Baskaran, Smits & Joubert 1987) and the boundary layer over a bump (Webster, DeGraaff & Eaton 1996). In Baskaran *et al.* (1987), the streamwise pressure gradient changes rapidly from adverse to favourable at the leading edge, and separation occurs downstream of the summit. An internal layer was found downstream of the leading edge. The flow of Webster *et al.* (1996) remains attached, its streamwise pressure gradient changes suddenly from adverse to favourable at both the leading and trailing edges and internal layers were identified downstream of these two locations. They considered signatures of internal layers as knee points in the wall-normal profiles of streamwise turbulence intensity. In these two studies, knee points emerge when the outer peak of streamwise turbulence intensity associated with upstream adverse pressure gradient decays rapidly under favourable pressure gradient and an inner peak is established as a result of the internal layer. Obviously, this process of knee-point formation is specific to the hill or bump type of flows in which the upstream strong adverse pressure gradient changes suddenly to favourable at the leading/trailing edges.

This paper describes an internal layer identified from an incompressible turbulent diffuser flow, as opposed to the internal layers previously identified from external boundary-layer flows. The present internal layer emerges in the relaxation zone downstream of a sharp variation in streamwise pressure gradient: from mildly favourable to strongly adverse, then weakly adverse. Unlike those in Baskaran *et al.* (1987) and Webster *et al.* (1996), the present internal layer does not display significant spreading into the central region of the flow. The flow in the region where the internal layer forms, exhibits certain characteristics similar to those observed in the C-type of Couette–Poiseuille turbulent flows.

Two laboratory incompressible diffuser flows have emerged in a number of fundamental and modelling studies on spatially developing complex internal turbulent flows, namely, the Azad diffuser (Azad 1996) and the Obi diffuser (Obi, Aoki & Masuda 1993). The Azad diffuser is an axisymmetric conical geometry with a total divergence angle of 8° and with fully developed pipe flow at the inlet. The inlet Reynolds number based on friction velocity and pipe diameter is 12 400. Extensive measurements have been performed on this flow by Okwuobi & Azad (1973), Trupp, Azad & Kassab (1986) and Azad & Kassab (1989), among others. They found that sudden application of an adverse pressure gradient at the diffuser throat affects the flow so drastically that the downstream mean and turbulent fields become unrecognizable in relation to the inlet condition. The Obi diffuser has an asymmetric planar configuration with a total expansion ratio of 4.7 and a single-sided deflection wall of 10° (see figure 1). The

inlet was designed to be a fully developed turbulent channel flow, though in some of the experiments this condition was not achieved. The inlet Reynolds number based on friction velocity and channel half-height is 500. Obi *et al.* (1993) studied the flow experimentally using a single-component laser-Doppler anemometer. Buice & Eaton (1997) made hot-wire and pulsed-wire measurements in the Obi diffuser. Lindgren, Tornblom & Johansson (2002) made measurements on a slightly modified geometry based on the Obi diffuser at a higher Reynolds number to study the control of flow separation. Lim & Choi (2004) performed shape optimization using the Obi diffuser as the base flow configuration. The Obi diffuser has also been used as a test flow in a number of computational studies. These include the Reynolds-averaged simulations of Durbin (1995) and Iaccarino (2001), as well as the large-eddy-simulation (LES) work of Kaltenbach *et al.* (1999) and Gravemeier (2005). Previous investigations in the Azad diffuser emphasized the process of instantaneous flow reversal (Azad 1996). Likewise, work in the Obi diffuser emphasized the unsteady process of separation on the lower deflected wall, e.g. see Kaltenbach *et al.* (1999). The focus of the present study is on the discovery of an internal layer over the upper flat wall of the Obi diffuser. This subject has eluded attention in the previous diffuser studies which have focused on separation and reattachment over the lower deflected wall.

Aside from the obvious outstanding issue of identifying internal layers in internal flows, further flow physics questions can be raised with reference to the conditions under which internal layers may form, about the growth rate of the internal layer, and about a possible connection between turbulent fluctuations inside the internal layer and identifiable large-scale motions in the central region of the flow. In addition, from the view point of basic fluid mechanics, it is of interest to query whether it is possible to relate the characteristics of the internal layer with any well-known fundamental equilibrium component flows. Furthermore, the original internal-layer concept proposed by Townsend (1965) requires further scrutiny. Can the internal layer be accurately described as a near-wall layer with turbulence energy equilibrium? Does the layer outside the internal layer develop as in the original unperturbed flow? Does the internal layer emerge right at the streamwise section of change? In this work, we attempt to address these questions using large-eddy simulation.

2. Notations and computational procedures

We consider incompressible fluid flow with constant density ρ in the Obi planar diffuser shown in figure 1. The unit length scale is h, corresponding to the inlet channel half-height. The two transitional curvatures between the parallel walls and the inclined wall have the same radius of 19.4. The origin of the coordinate system is at the intersection of the deflected wall and the lower inlet channel wall. The curvature centre associated with the upstream curved section is located at ($x=-1.7$, $y=-19.4$). The curvature center of the downstream curved section is at ($x=43.7$, $y=12.0$). The inlet plane is located at $x=-5$, and the outlet plane at $x=100$.

Mass and momentum conservation equations are

$$\operatorname{div} \boldsymbol{u} = \boldsymbol{0}, \tag{1}$$

$$\frac{\partial \boldsymbol{u}}{\partial t} + \operatorname{div}(\boldsymbol{u}\,\boldsymbol{u}) = -\frac{1}{\rho}\operatorname{grad} p + \operatorname{div}\left\{\frac{1}{\mathrm{Re}}[\operatorname{grad}\boldsymbol{u} + (\operatorname{grad}\boldsymbol{u})^{\mathscr{T}}]\right\}, \tag{2}$$

where $\boldsymbol{u}$ is the velocity vector with Cartesian components (u, v, w) or u_i, $i=1, 2, 3$. Superscript '$\mathscr{T}$' denotes transpose. The corresponding grid-filtered large-eddy

simulation equations are

$$\operatorname{div} \overline{\boldsymbol{u}} = 0, \tag{3}$$

$$\frac{\partial \overline{\boldsymbol{u}}}{\partial t} + \operatorname{div}(\overline{\boldsymbol{u}}\,\overline{\boldsymbol{u}}) = -\frac{1}{\rho}\operatorname{grad}\overline{p} + \operatorname{div}\left\{\frac{1}{\mathrm{Re}}[\operatorname{grad}\overline{\boldsymbol{u}} + (\operatorname{grad}\overline{\boldsymbol{u}})^{\mathscr{T}}]\right\} + \operatorname{div}(-\tau) + \varepsilon, \tag{4}$$

where an overbar denotes the filtered variable. The term ε appearing in (4) represents an error caused by the general filtering operation not commuting with differentiation, and is neglected in this work (or absorbed into τ). The term τ is the subgrid-scale stress tensor with Cartesian components τ_{ij}, $i, j = 1, 2, 3$. In this paper, τ_{ij} is parameterized using the Smagorinsky model together with a slightly modified implementation of the dynamic procedure (Germano *et al.* 1991). Details of the subgrid-scale stress model equations and the associated filtering operation can be found in Mahesh, Constantinescu & Moin (2004), and are not repeated here.

The unit velocity scale is defined as the friction velocity u^* at the inlet. This then defines the unit time scale as $h/u^*_{x=-5}$. The Reynolds number Re based on the unit length h and unit velocity $u^*_{x=-5}$ is 500. As in previous studies of the Obi diffuser (e.g. Buice & Eaton 1997; Kaltenbach *et al.* 1999), the majority of the results in this paper were normalized by the inlet bulk velocity u_b defined as the area-averaged mean streamwise velocity at the $x = -5$ station. Time-averaging and averaging over the spanwise homogeneous direction are represented by $\langle\cdot\rangle$.

The two-point correlation coefficient with spatial and temporal separations is defined as

$$R_{ij}(x, y, z - z', t - t', x', y') = \frac{\langle \overline{u}_i'(x, y, z, t)\overline{u}_j'(x', y', z', t')\rangle}{\overline{u}_{i,rms}'(x, y)\overline{u}_{j,rms}'(x', y')} \qquad (i, j = 1, 2, 3). \tag{5}$$

For the two homogeneous dimensions z and t, only relative separation is significant.

The wall static pressure coefficient and skin friction coefficient are evaluated as

$$C_{pw} = \frac{\langle \overline{p}\rangle_{wall} - \langle \overline{p}\rangle_{wall,x=-5}}{\frac{1}{2}\rho u_b^2}, \qquad C_f = \frac{\langle wall\ shear\ stress\rangle}{\frac{1}{2}\rho u_b^2}. \tag{6}$$

Evaluation of power spectra in this paper follows the procedure described in Choi & Moin (1990).

The two-dimensional rate of deformation tensor for mean flow is

$$S_{ij} = \frac{1}{2}\left(\frac{\partial\langle\overline{u}_i\rangle}{\partial x_j} + \frac{\partial\langle\overline{u}_j\rangle}{\partial x_i}\right) \qquad (i, j = 1, 2). \tag{7}$$

The first eigenvalue for S_{ij} is

$$\lambda_1 = \frac{S_{11} + S_{22}}{2} + \sqrt{\left(\frac{S_{11} - S_{22}}{2}\right)^2 + S_{12}^2}, \tag{8}$$

and the principal axis of S_{ij} associated with λ_1 makes an angle ϕ with respect to the x-axis,

$$\tan\phi_1 = \frac{\lambda_1 - S_{11}}{S_{12}}. \tag{9}$$

The numerical methodology used to solve the filtered continuity and momentum equations is the unstructured fractional step method for large-eddy simulation in complex geometries of Mahesh *et al.* (2004). Their method defines all independent variables at the control volume cell center as in the collocated implicit formulation

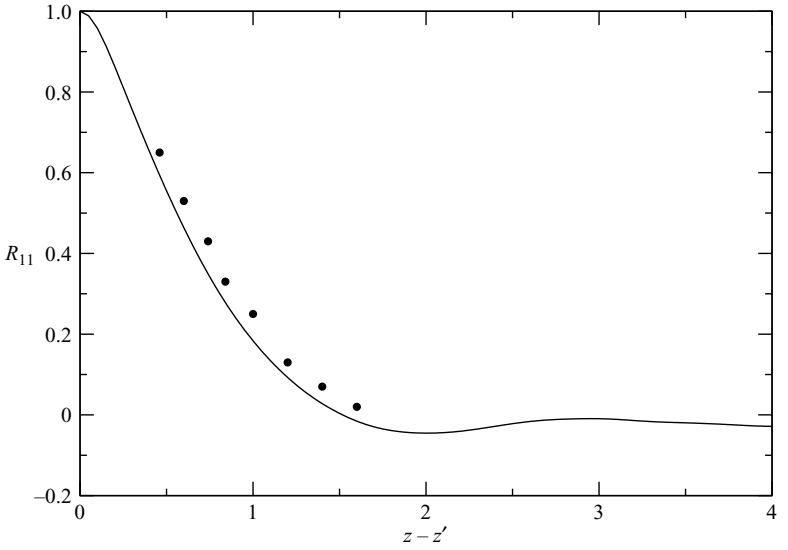

FIGURE 2. Two-point correlation coefficient $R_{11}(x=35.6, y=-0.4, z-z', t-t'=0, x'=x, y'=y)$ as a function of spanwise separation $z-z'$. ●, Buice & Eaton (1997); solid line, present LES.

developed by Kim & Choi (2000). An implicit second-order Crank–Nicolson scheme is used for both convection and viscous terms. For further details about the numerical algorithm, see Mahesh *et al.* (2004). The actual parallel computer program developed based on this method is named CDP after the late Dr Charles David Pierce of the Center for Turbulence Research, Stanford University.

The spanwise dimension of the computational domain is $8h$, taken to be the widest value adopted in the simulation of Kaltenbach *et al.* (1999). The computed spanwise two-point correlation coefficient R_{11} at $x=35.6$ and $y=-0.4$ is plotted together with the experimental data of Buice & Eaton (1997) in figure 2. The comparison is satisfactory, and the profile also indicates the adequacy of the chosen domain width.

Velocities at the inflow boundary plane, $x=-5$, are from a separate LES of a fully developed channel flow at $Re=500$. The channel length in the separate LES is 12, its width and height are the same as the diffuser inlet section. Resolution used in this channel LES is 128^3 with the first layer of cell centres located at 0.000487 away from the wall. The numerical algorithm for the channel LES is the second-order staggered fractional step method of Pierce & Moin (2004). The mean and r.m.s. velocities obtained from the channel LES are in good agreement with the DNS data of Moser, Kim & Mansour (1999). The channel velocities at one selected plane were saved for 20 time units at time intervals of 0.002. The velocity signals were interpolated temporally and spatially in the unstructured collocated diffuser simulation for inlet boundary condition. The time duration of the inflow data sequence is long enough to allow a fluid particle to be convected approximately 100 length units in the streamwise direction. When the end of the saved data sequence is reached, the signals are recycled. In the present diffuser simulation, the saved inlet-channel velocity signals were rescaled to match the $\overline{u}'_{rms}$ distribution of Buice & Eaton (1997), similar to the procedure used by Schlüter, Pitsch & Moin (2004) and Keating *et al.* (2004). This is because it was felt that in order to compare the diffuser LES results with the experiments of Buice & Eaton (1997), the inflow statistics should match the experiment as closely as possible. The drawback is that turbulence structures will be slightly distorted at

the inlet. However, we found that the interpolations in time, space and rescaling of $\overline{u}'_{rms}$ at the inlet resulted in small changes in the energy spectrum of $\overline{u}$ at ($x = -4.99$, $y = 1.8$, $z = 1$) compared to that of the originally saved fully developed channel flow velocity signals. A simulation without rescaling the inlet channel profiles was also performed.

A periodic boundary condition was applied in the spanwise z-direction and no-slip boundary conditions were applied on the walls. At the exit plane, a convective boundary condition was used (see Kaltenbach *et al.* 1999; Pierce & Moin 2004).

Simulations were performed on two sets of hexahedral meshes. The fine mesh has $590(x) \times 100(y) \times 110(z)$ control volume cells. At the inlet, the first layer of cell centres is located at 0.0013 away from the two channel walls. Along the streamwise direction, the cell length is 0.083. At $x = 20$, the first layer of cell centres is located at 0.0037 below the upper wall, and the cell length is 0.1187. The coarse mesh has $360(x) \times 80(y) \times 80(z)$ control volume cells. At the inlet, the first layer of cell centres is located at 0.0055 away from the two channel walls. Along the streamwise direction, the cell length is 0.11. At $x = 20$, the first layer of cell centres is located at 0.033 below the upper wall, and near the upper wall the cell length is 0.175. These mesh spacings can be translated into wall units using the skin friction results and the value of characteristic Reynolds number. Effects of grid resolution and the subgrid-scale stress model on predicted mean and r.m.s. velocities were studied. It was found that for the coarse resolution, application of the subgrid-scale stress model improves predictions of $\langle\overline{u}\rangle/u_b$ and $\overline{u}'_{rms}/u_b$. With the model applied, the mean velocity $\langle\overline{u}\rangle/u_b$ shows small differences between the two resolutions, and agrees well with the experimental data of Buice & Eaton (1997). The results to be presented in the next section are from the fine-mesh simulation. The computed inlet bulk velocity u_b used in the normalization of results is 18.19.

The computation was carried out on parallel computers using 128 processors. The time step was fixed to be $\Delta t = 0.0013$. Initial velocities were set to zero across the entire field. The flow was allowed to evolve for 120 time units (approximately 6 flow through times) and reach a statistically steady state. Velocity fields at selected (y, z)-planes were then saved periodically every $100\Delta t$ for a duration of 100 time units for post-processing. Mean velocity and turbulence intensities were sampled at every time step during the simulation to collect statistics. For the calculation of power spectra estimation 32 000 velocity samples were saved at 25 selected spatial locations at every time step. All 25 recorded points are located in the $z = 1$ plane. Notations related to power spectrum computation follow strictly those in Choi & Moin (1990).

3. Internal layer definition and identification

Townsend (1965) considered the response of a deep self-preserving turbulent boundary layer to sudden change in surface roughness. He postulated that an inner equilibrium layer with logarithmic mean streamwise velocity profile emerges downstream of the perturbation. 'Equilibrium' is in the sense of Townsend (1961), which refers to the equilibrium existing between local rates of turbulence energy production and dissipation. Bradshaw & Galea (1967) extended the development of Townsend and proposed that the internal layer may be identified by plotting total pressure against streamfunction for various values of streamwise locations. Outside the internal layer, the total pressure on a streamline continues to change slowly as in the upstream flow, whereas in the internal layer under adverse pressure gradient, the total pressure increases along a streamline. Antonia & Luxton (1971) measured

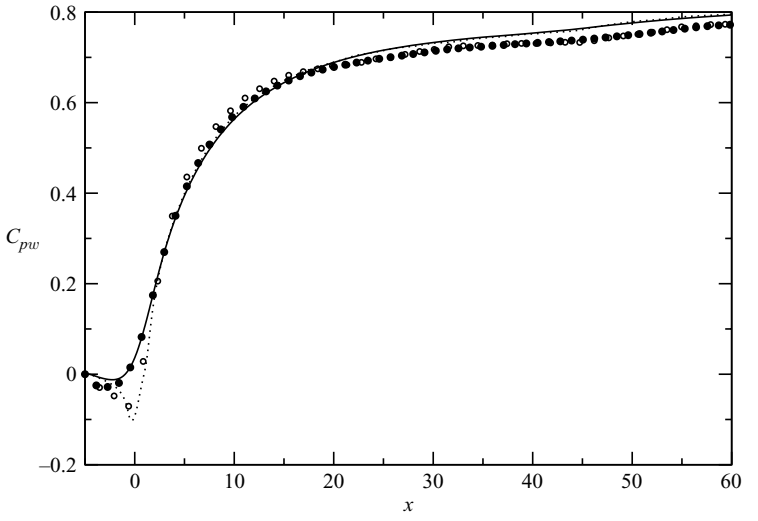

FIGURE 3. Wall static pressure coefficient C_{pw}. Kaltenbach *et al.* (1999): ○, lower wall; ●, upper wall. Present LES: dotted line, lower wall; solid line, upper wall.

the response of a turbulent boundary layer to a smooth-to-rough change in surface condition. They reported that the internal layer flow near the wall downstream of the perturbation is not in energy equilibrium as suggested by Townsend.

We propose to define the internal layer as a near-wall attached layer with inflectional mean velocity gradient, emerging downstream of imposed perturbations on the upstream flow.

In the Obi diffuser flow, an imposed perturbation arises from the sharp adverse pressure gradient downstream of the diffuser throat. Planar and conical diffusers have broadly similar wall static pressure distributions. A mildly favourable pressure gradient turns to a sharply adverse pressure gradient at the diffuser throat, followed by a gradual decrease in the magnitude of the adverse pressure gradient further downstream. Such similarity can be appreciated by comparing the C_{pw} results for the Obi diffuser in figure 3 with figure 4 of Okwuobi & Azad (1973) for the axisymmetric Azad diffuser. In figure 3, the change from strongly adverse to weakly adverse pressure gradient starts near $x = 10$, and in the experiment of Okwuobi & Azad (1973) similar transition takes place approximately 8 pipe radii downstream of the throat, though the levelling off of C_{pw} is not as distinct as in the Obi diffuser. This pattern of C_{pw} for incompressible diffuser flows may be contrasted with the behaviour of C_{pw} found in the hill/bump flows of Baskaran *et al.* (1987) and Webster *et al.* (1996). In Webster *et al.* (1996) there are two adverse to favourable pressure gradient changes where signatures of internal layers emerge. The magnitude of their favourable pressure gradient decreases further downstream of the trailing edge. The diffuser flow and the bump flow both experience sharp variation in streamwise pressure gradient followed by downstream relaxation. The difference is that the signs of the sudden changes are opposite. Given that the internal layer exists in the scenario where C_{pw} is from adverse to favourable, a query which naturally presents itself is whether an internal layer can be found in the other scenario.

Inflectional mean streamwise velocity and its wall-normal gradient are shown in figures 4 and 5. On the scales adopted in the figures, mean velocity profiles near the top flat wall exhibit a nearly discontinuous abrupt change of curvature at $y \approx 1.8$

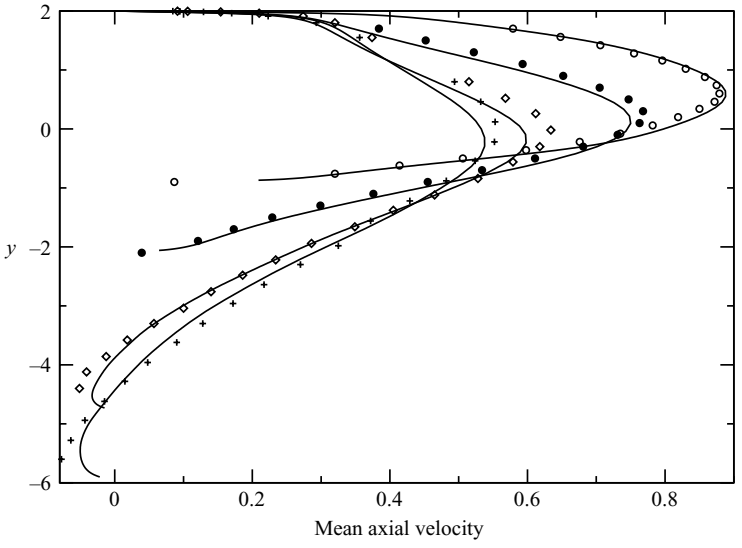

FIGURE 4. $\langle\overline{u}\rangle/u_b$ versus y. Symbols are from Buice & Eaton (1997) and lines are present LES. ○, $x = 5.18$; ●, $x = 11.96$; ◇, $x = 27.1$; +, $x = 33.86$.

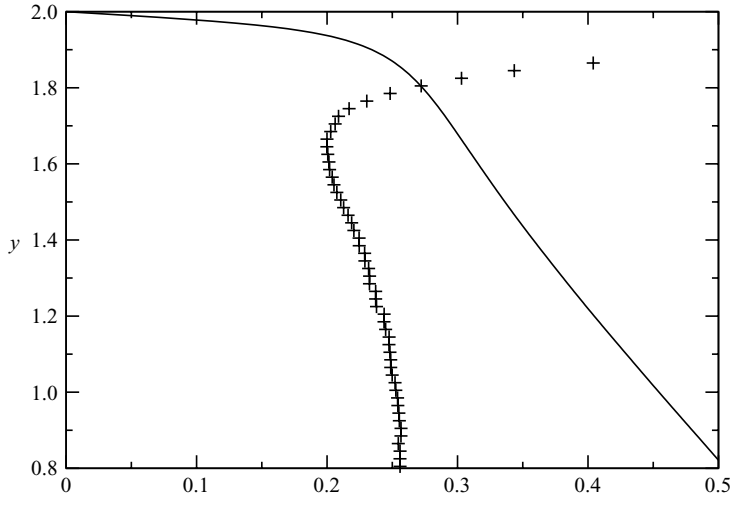

FIGURE 5. Mean streamwise velocity and its gradient near the upper wall at $x = 20$. Solid line, $\overline{u}/u_b$; +, $-1/u_b\partial\overline{u}/\partial y$.

for those streamwise stations located within the range from $x = 11.96$ to 38.4. In addition, along the wall-normal direction from the abrupt change to approximately $y = 0$, $\langle\overline{u}\rangle/u_b$ displays linear slopes at these streamwise stations. In this paper, we will refer to this region as the flow outside the internal layer, the outer flow, or the core region. The linearity of mean velocity in the core region is significant because it implies that, for the outer flow, the velocity difference is only a function of distance (not necessarily linear) to the wall, thereby satisfying a crucial condition in Millikan's reasoning (velocity defect law) for the existence of a logarithmic velocity profile in the overlap region for the flow underneath the core flow. The original argument is that at a reasonably large distance from the wall, the viscosity factor should no longer

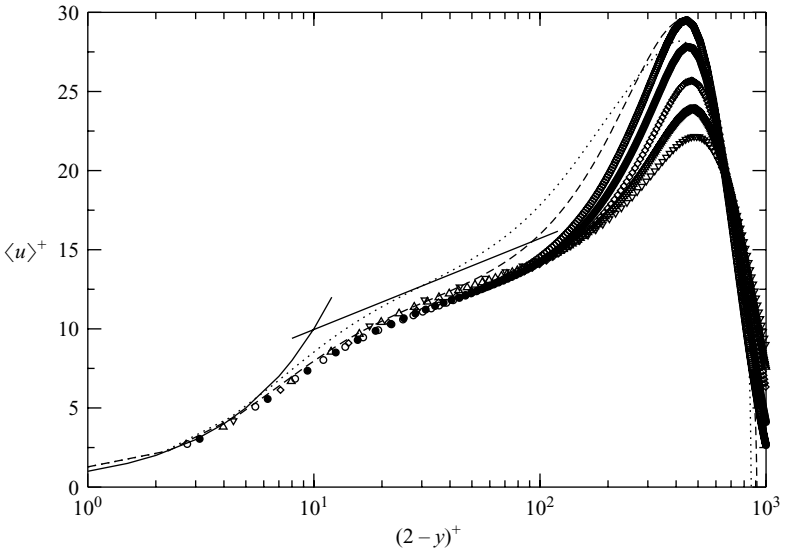

FIGURE 6. $(2-y)^+$ versus $\langle\overline{u}\rangle^+$. dotted line, $x=6.4$; dashed line, $x=10.4$; ○, $x=18.4$; ●, $x=22.4$; ◇, $x=26.4$; △, $x=30.4$; ▽, $x=34.4$; solid lines are $\langle\overline{u}\rangle^+=y^+$ and $\langle\overline{u}\rangle^+=2.5\ln y^+ + 4.2$.

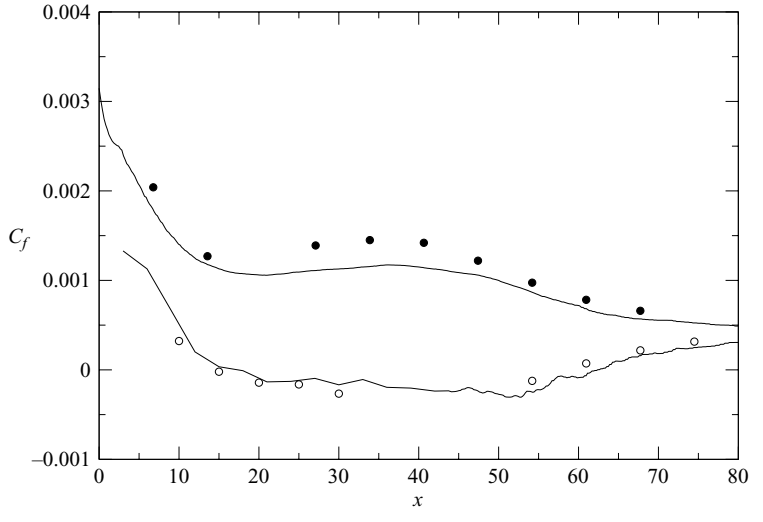

FIGURE 7. Skin friction coefficient. Buice & Eaton (1997): ○, lower wall; ●, upper flat wall; solid lines are from the present LES.

be predominant in determining the velocity profile. Velocity differences in this region should therefore depend only on geometrical factors. We therefore may argue that underneath the core flow, the mean velocity profiles should be logarithmic.

The above prediction is put to the test in figure 6 by plotting the mean velocity $\langle\overline{u}\rangle^+$ against wall distance $(2-y)^+$ in wall units. Using the friction velocity suggested in figure 7, it can be shown that $y=1.8$ corresponds to approximately 45 wall units at the last five x locations ($18.4 \leqslant x \leqslant 34.4$). From $(2-y)^+=20$ to 80, the $\langle\overline{u}\rangle^+$ profiles at these five streamwise stations collapse onto a logarithmic curve with the

well-known slope of 1/0.4. Very close to the wall, $(2-y)^+ < 10$, the usual law of the wall is satisfied. One of the signatures of the present internal layer is that the mean velocity obeys the self-similar log law and law of the wall inside the internal layer, and varies linearly with distance from the wall outside the internal layer. It may be possible to further collapse the $\langle\overline{u}\rangle/u_b$ profiles at different streamwise locations outside the internal layer in the core region of the flow. For scaling of mean velocity in adverse pressure gradient boundary layers, see the work of Na & Moin (1998), Skote & Henningson (2002) and references therein. Scaling in simple equilibrium internal flows was discussed in Nakabayashi, Kitoh & Katoh (2004).

4. Conditions of internal layer occurrence

Skin friction coefficient C_f over the upper flat wall in the Obi diffuser displays a long plateau extending from $x = 15$ to 45 (figure 7). The plateau is bound by a sharp drop from $x = 0$ to 10 upstream and a more gradual decline downstream of $x = 45$. In the plateau region, friction velocity is approximately 0.43, and 1 viscous wall unit corresponds to $0.0047h$. A broadly similar streamwise variation of C_f exists in the Azad diffuser (see figure 17 of Azad 1996). However, in the Azad diffuser, the sharp drop of C_f near the diffuser throat is followed by an additional slower decrease rather than a distinct plateau. In Webster *et al.* (1996), two sudden jumps in C_f are found at the locations where the pressure gradient changes from adverse to favourable. Downstream of their trailing edge, C_f settles into a minor descending slope and the signature of the internal layer is distinct in this region. Wu & Squires (1998) argued that an abrupt increase in C_f implies quasi-step changes in the near-wall mean velocity gradient. Thus, production terms which are directly dependent on this gradient in the transport equations for second-order turbulence statistics will be expected to show large increases in the near-wall region, for example, streamwise intensity. The proposition of Wu & Squires (1998) that a quasi-step increase in C_f selectively modifies near-wall shear production of turbulent stresses and leads to signatures of an internal layer explains well the internal layers identified in Webster *et al.* (1996) and Baskaran *et al.* (1987), but is not directly applicable in the present diffuser flow. This is because near the upper flat wall of the Obi diffuser, there is no quasi-step increase in C_f. Instead, C_f has a prolonged plateau which is preceded by a rapid decrease. Although the overall trend of C_f in the Obi diffuser is drastically different from that in the Webster bump, both flows nevertheless show regions of stabilized positive skin friction downstream of sections of sudden change. Again, the signs of the sudden changes are opposite. The stabilized C_f in the relaxation region suggests a newly established level of the near-wall mean velocity gradient, which may be the driving factor in the formation of an internal layer. Obviously, if the sharp drop in C_f on the upper wall of the Obi diffuser is severe enough to cause separation, there can be no internal layer. We therefore propose to view a quasi-step change in skin friction followed by stabilization as a necessary condition for the occurrence of an internal layer, provided that C_f remains positive after the perturbation.

5. Similarity with other equilibrium flow

In the region of $1 < y < 2$ and $18 < x < 38$, the present mean velocity profiles exhibit certain similar characteristics to those in the C-type of Couette–Poiseuille turbulent flows measured by Nakabayashi *et al.* (2004), which can be observed by comparing figures 5 and 8 with the sketch shown in figure 9. The inflectional point where the

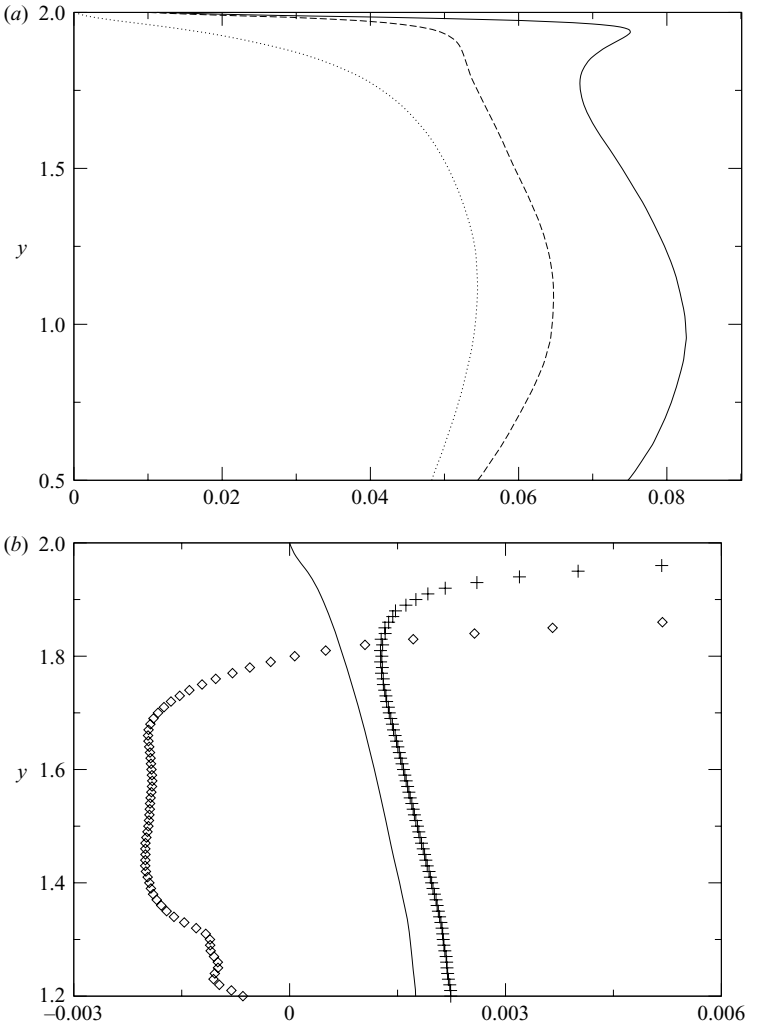

FIGURE 8. Second-order turbulent statistics near the upper wall at $x = 20$. (*a*) solid line, $\overline{u}'_{rms}/u_b$; dotted line, $\overline{v}_{rms}'/u_b$; dashed line, $\overline{w}_{rms}'/u_b$; (*b*) solid line, $\langle\overline{u}'\overline{v}'\rangle/u_b^2$; +, total shear stress; ◇, wall-normal gradient of total shear stress.

second-order wall-normal mean velocity gradient changes sign is less apparent from the distribution of $\langle\overline{u}\rangle/u_b$ in the present diffuser flow. However, the profile of $\partial\langle\overline{u}\rangle/\partial y$ shown in figure 5 clearly demonstrates that the inflection is located at approximately $y = 1.7$. The effect on mean velocity of the lower moving wall in the C-type of flow is mimicked in the present diffuser flow by the high-speed fluid beyond the core region, i.e. $y < 1$. Thus, if the C-type of Couette–Poiseuille turbulent flows can be considered approximately as a distant prototype for the Obi diffuser flow in the region of $1 < y < 2$ and $18 < x < 38$, the linearly varying high-speed fluid flow away from the top wall is then one of the driving components in the internal-layer formation process because it provides the necessary mechanism for a mean velocity inflection in this particular flow.

The notion that the present internal layer, together with its surrounding environment, bears a certain resemblance to the fundamental C-type of Couette–Poiseuille turbulent flows is reinforced by considering the characteristics of second-order

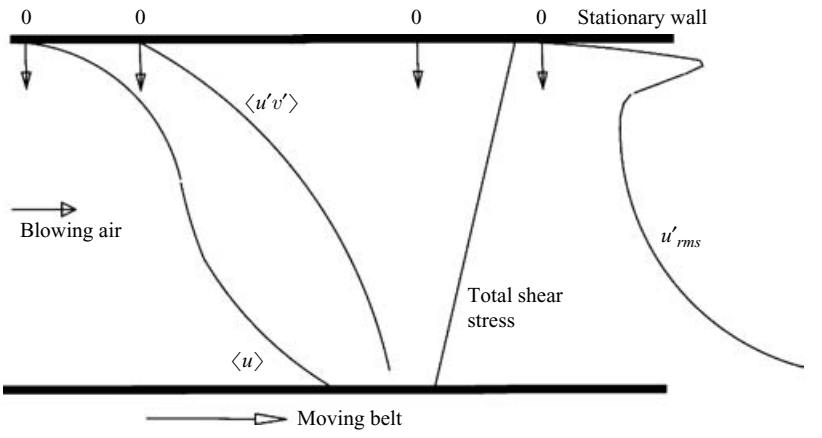

FIGURE 9. Sketch of the C-type of Couette–Poiseuille turbulent flows, based on the experimental data of Nakabayashi *et al.* (2004).

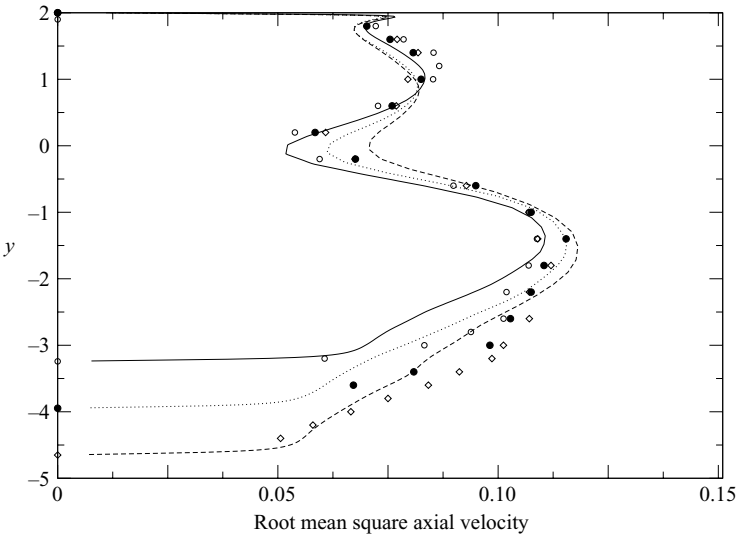

FIGURE 10. $\overline{u}'_{rms}/u_b$ versus y. Symbols are from Obi *et al.* (1993) and lines are present LES. ○ solid, $x = 18.4$; ● dotted, $x = 22.4$; ◇ dashed, $x = 26.4$.

turbulence statistics in these two flows. The $\overline{u}_{rms}{}'$ profiles close to the top wall in figures 8 and 10 may be compared with figure 14 of Nakabayashi *et al.* (2004). The valley between the inner and outer $\overline{u}_{rms}{}'$ peaks in the present discussion has been termed a plateau region in Nakabayashi *et al.* Reynolds shear stress similarity between these two types of flow can be appreciated by comparing the $\langle u'v' \rangle$ profile in figure 8 with those in figure 4 of Nakabayashi *et al.* (2004). Note the absence of an inflection in the Reynolds shear stress profiles for both flow. Apparently, the total shear stress in the present diffuser flow at $x = 20$ close to the top wall has different behaviour from that in the C-type of Couette–Poiseuille turbulent flows. This reflects the fact that the present flow is not one-dimensional and fully developed, as assumed in the C-type of Couette–Poiseuille turbulent flows. The wall-normal gradient of total shear stress shown in figure 8 also serves as a measure for identification of an internal

layer. In adverse pressure gradient boundary-layer flows, it is approximately equal to the streamwise gradient of total pressure. Outside the internal layer, the total pressure on a streamline continues to change slowly as in the upstream flow, whereas inside the internal layer under adverse pressure gradient, the total pressure increases along a streamline, at the wall being equal to the static pressure. In the present flow, the location at which the total shear stress gradient changes sign serves as one of the markers for the edge of the internal layer.

6. Connection of internal layer with outer flow

Antonia & Luxton (1971) reported that the structure of the flow outside their internal layer does not seem to be affected by the new surface condition, except for a small streamline displacement. Baskaran *et al.* (1987) also found from their bump experiment that flow outside the internal layer behaves as free turbulent flow affected by a wall constraint. In this work, we primarily use two-point correlation with spatial separation and temporal delay to gain insight into this issue.

Figure 11 compares the contour maps of $R_{12}(x=16, y, z-z'=0, t-t'=0, x'=x, y')$ in a region near the upper wall $1<y<2$, where an internal layer exists with its inlet counterpart $R_{12}(x=-5, y, z-z'=0, t-t'=0, x'=x, y')$. At $x=16$ outside the internal layer for $1<y<1.8$, the correlation reaches peak values at zero wall-normal separation $y=y'$. The streamwise fluctuation $\overline{u}'$ in the core region is strongly correlated with wall-normal fluctuation $\overline{v}'$ at the same location. The magnitude of the peaks also increases toward the lower left-hand corner $y=y'=1$ where the local maximum of Reynolds shear stress is located under the effect of adverse pressure gradient. In the contour map, a neck forms between $y=1.75$ and 1.85 suggesting different correlation characteristics of R_{12} inside and outside the internal layer. Inside the internal layer, the peaks of $R_{12}(x=16, y, z-z'=0, t-t'=0, x'=x, y')$ are displaced away from zero wall-normal separation, i.e. $y-y'>0$. The streamwise fluctuation $\overline{u}'$ inside the internal layer is more strongly correlated with $\overline{v}'$ further away from the wall. At the inlet plane the correlation map does not show a distinct neck, though a slight bending toward positive separation $y-y'>0$ is visible for $y>1.9$. The correlation reaches a local maximum for each y at zero wall-normal separation, and the peak values decrease monotonically along the 45° line connecting the upper right- and the lower left-hand corners. The correlation coefficient map of R_{12} clearly suggests a distinct separation in the behaviours of large-eddy motions inside and outside the internal layer.

The next point to be discussed is the degree of correlation between the streamwise fluctuation $\overline{u}'$ inside the internal layer and $\overline{u}'$ away from the wall. This is addressed through consideration of R_{11} with finite streamwise separation, variable wall-normal separation, and also at variable time delay. Contour maps of the two-point correlation coefficient $R_{11}(x=33.86, y, z-z'=0, t-t', x'=35.60, y')$ at nine sequentially increasing time delays are shown in figure 12. At zero time delay, as indicated by the shape of the $R_{11}=0.5$ contour line, the streamwise fluctuations inside the internal layer $y>1.8$ at the upstream station $x=33.86$ have a relatively high degree of correlation with streamwise fluctuations away from the wall within $1.3<y<1.8$ at the downstream station of $x'=35.60$. If long streamwise streaky structures were dominant inside the internal layer, the coefficient R_{11} at zero time delay should have shown a high degree of correlation between $\overline{u}'$ in $y>1.8$ at the upstream station with $\overline{u}'$ at similar y' coordinates at the downstream station. We also found from visualization studies that the long near-wall streamwise streaks coming from the upstream channel are destroyed at the throat of the diffuser. The results at zero time delay are consistent with the

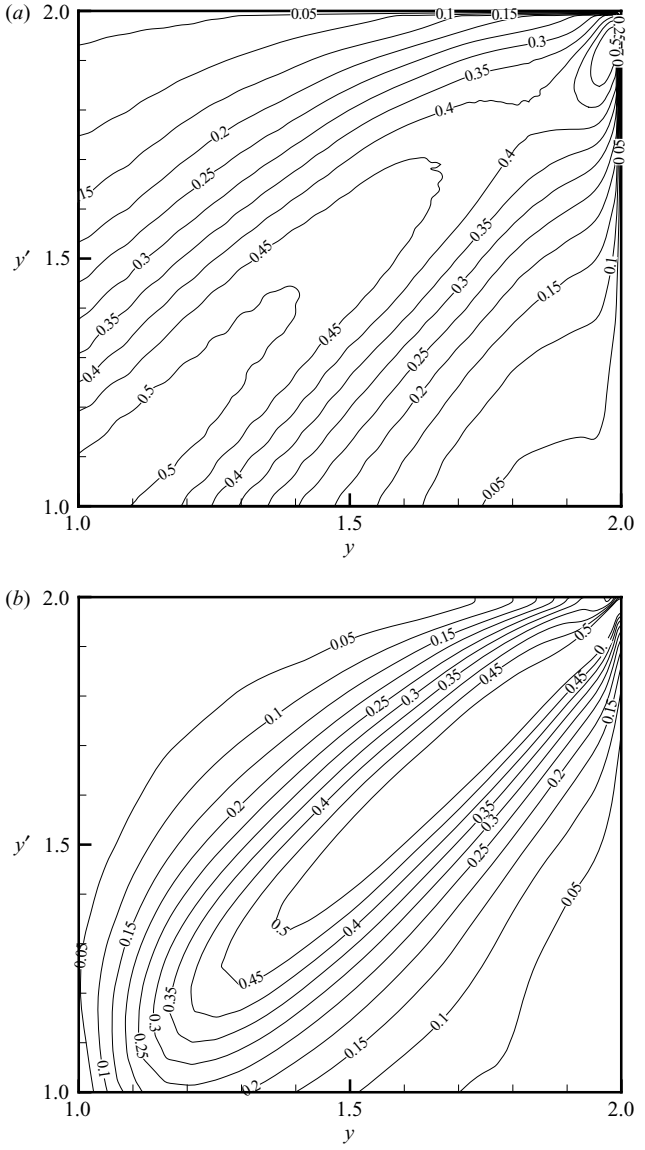

FIGURE 11. Contours of two-point correlation coefficient R_{12} with wall-normal separations. (*a*) $R_{12}(x=16, y, z-z'=0, t-t'=0, x'=x, y')$; (*b*) inflow plane $R_{12}(x=-5, y, z-z'=0, t-t'=0, x'=x, y')$.

well-established hairpin eddy structure in turbulent channel and boundary-layer flows. Upstream $\overline{u}'$ inside the internal layer and downstream $\overline{u}'$ in the core region belong to the tail and leg elements of one hairpin eddy structure, respectively. At 0.26 time delay, the correlation coefficient reaches a global peak value of 0.75 for all the nine time delays considered, and the contours are aligned with the 45° diagonal line in the (y, y')-coordinate system. The upstream $\overline{u}'$ is most strongly correlated with downstream $\overline{u}'$ with the same wall-normal coordinate at this optimum time delay, suggesting a simple translation of the eddy structure in the streamwise direction. The eddy convection velocity of $0.37u_b$ calculated based on $(x'-x)/(t'-t)u_b$ is

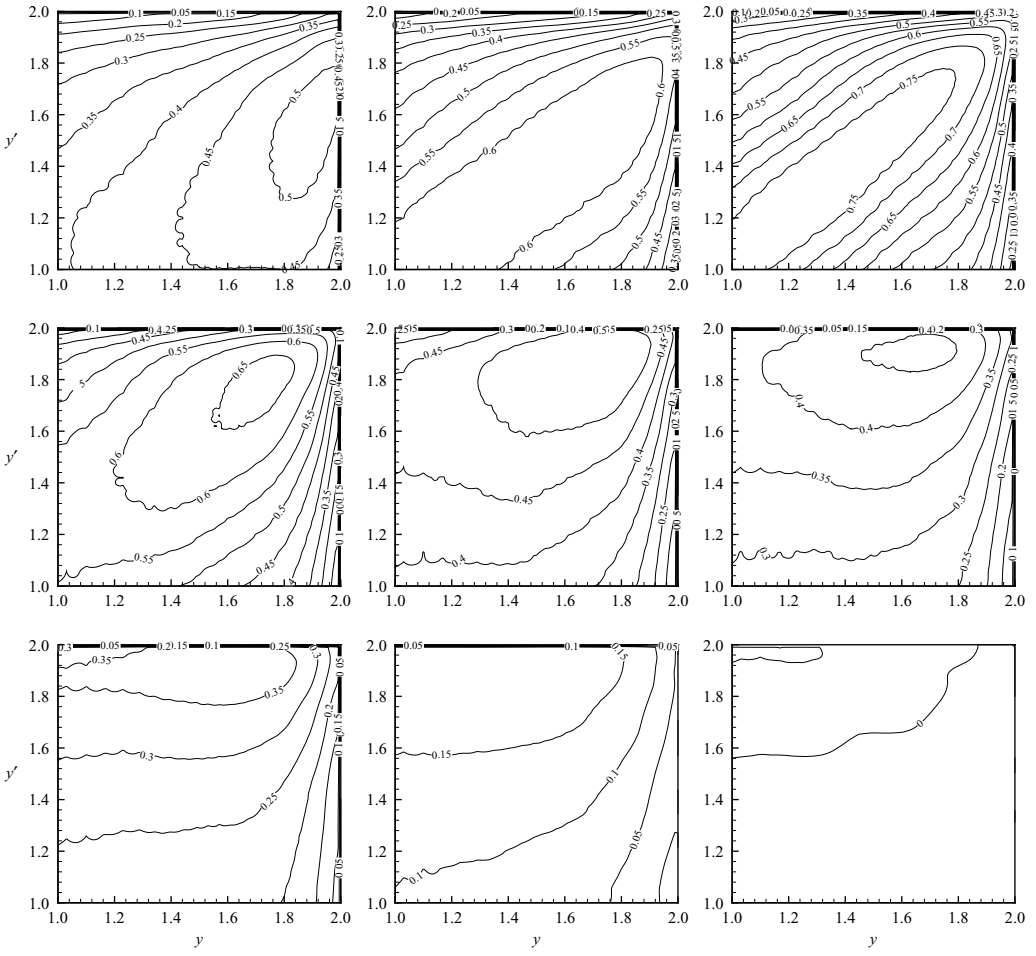

FIGURE 12. Two-point correlation coefficient $R_{11}(x = 33.86, y, z - z' = 0, t - t', x' = 35.60, y')$ with finite streamwise and wall-normal separations at a certain time delay. From the upper left-hand figure to the lower right-hand figure sequentially, the time delay $t' - t$ is 0, 0.13, 0.26, 0.39, 0.52, 0.65, 0.78, 1.3, 1.46.

nearly the same as the mean streamwise velocity in this region. Thus, the large eddies are convected downstream by the average streamwise velocity. Large eddies are also strained along the principal axis of the rate of deformation tensor as they move downstream. At the long time delay of 0.78, the contour line with local peak correlation value of 0.35 has a flattened loop shape nearly parallel to the horizontal y-axis. This suggests that at the given time delay, near-wall streamwise fluctuations at the downstream station of $x' = 35.60$ are more strongly correlated with streamwise fluctuations away from the wall at the upstream station $x = 33.86$.

Figure 13 shows Reynolds decomposed instantaneous fluctuating velocity vectors at $t = 200$ over the (x, y)-plane at $z = 1$. Inside the internal layer $(1.8 < y < 2)$, the fluctuating velocities reach local peak values in the central region. Near the outer edge of the internal layer they drop approximately to zero, forming a rather easily recognizable boundary between the internal layer and the outer flow. A distinct feature associated with the outer flow can also be seen in figure 13. From $x = 20.5$ to 24.5, there exists a layer of wavy fluctuating velocity vectors pointing toward the upstream

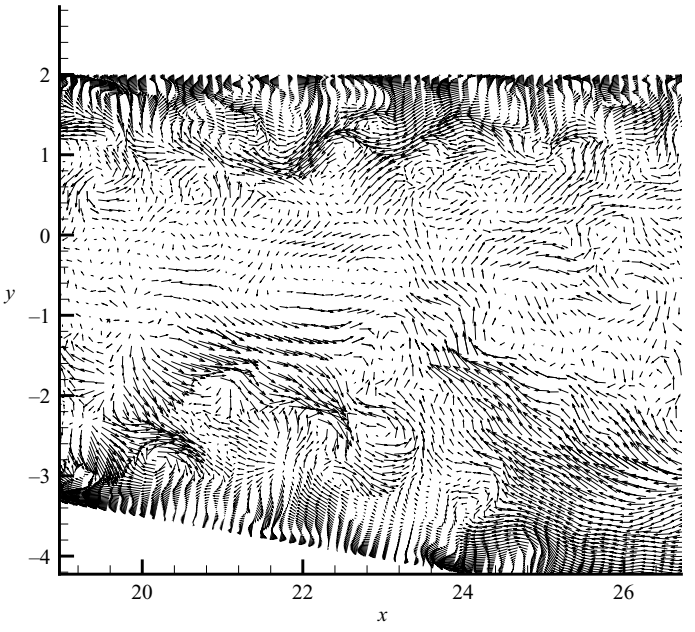

FIGURE 13. Instantaneous fluctuating velocity vectors over the $z = 1$ plane at $t = 200$.

direction. We may call it a stream. At $x = 22$, the wall-normal position of the stream is at $y \approx 1$. It is found that the spanwise extent of the stream is approximately 1. The magnitude of the fluctuating velocity $\overline{u}'$ in the stream is larger than the corresponding local turbulence intensity $\overline{u}'_{rms}$. The direction of a similar stream at a different instant may also point downstream instead of upstream. On the core flow side of the stream (smaller y-coordinate), well-defined spanwise vortices exist. It is possible that these spanwise vortices are related to the mean velocity inflection characteristic outside the internal layer. This is analogous to the situation in a plane mixing layer where an inflectional streamwise velocity profile results in a sequence of spanwise vortices as the flow develops either temporarily or spatially. Figure 14 presents Galilean decomposed fluctuating velocity vectors at the same time and location as in figure 13. The constant convection velocity u_c used in the Galilean decomposition is $0.5u_b$. At approximately $y = 1$, a string of well-defined spanwise vortices are revealed by the Galilean decomposition. Apparently, these vortices are convected downstream at a speed of $0.5u_b$; but unlike the counter-rotating vortex pairs shown in figure 13, these vortices all have the same counterclockwise swirl direction. The vortices identified from the Galilean decomposed velocity vector fields in Adrian, Christensen & Liu (2000) also exhibit the same sense of swirling.

7. Additional properties of the internal layer

Wu & Durbin (2001) reported direct numerical simulation of wake migration in a turbine passage channel. They found that circular vortex tubes aligned in the principal direction of the mean rate of deformation tensor emerge as the turbine geometry varies in the streamwise direction. Streamwise expansion of the Obi diffuser may produce similar effects. For this reason, the principal directions ϕ_1 of the mean rate of the deformation tensor as a function of y at various x stations are plotted in figure 15. Close to the inlet channel, ϕ_1 is nearly $-45°$ throughout the upper half-channel

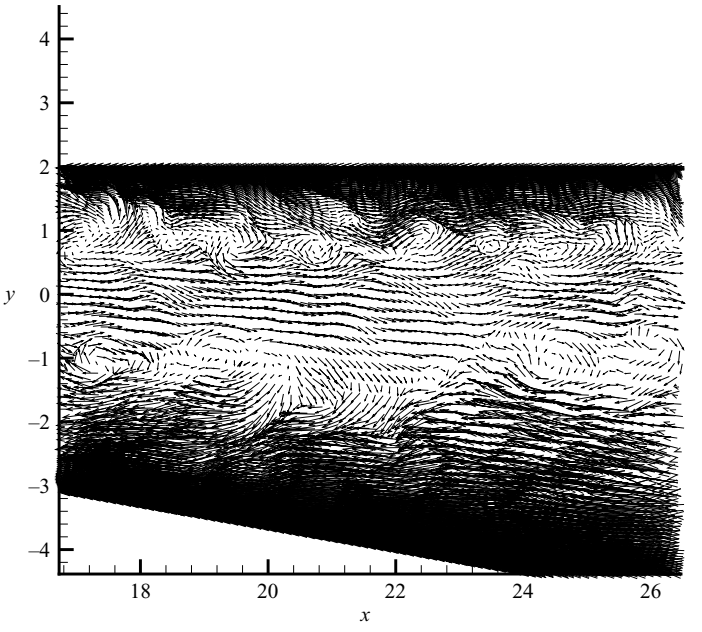

FIGURE 14. Instantaneous fluctuating velocity vectors over the $z = 1$ plane at $t = 200$ by Galilean decomposition with $u_C = 0.5u_b$.

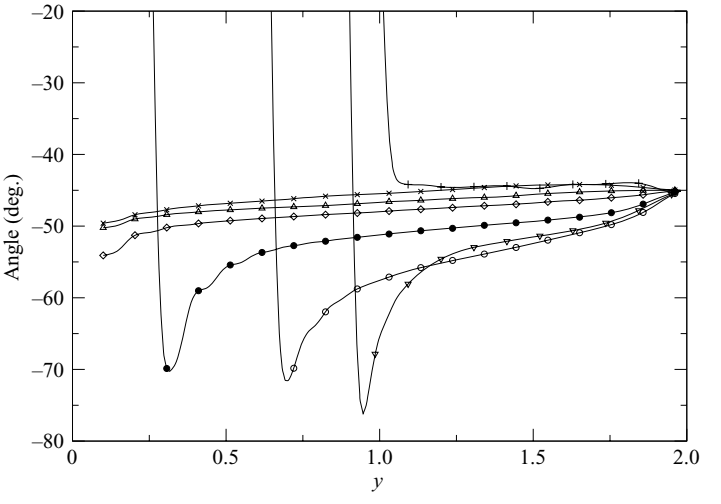

FIGURE 15. Principal direction ϕ_1 of the mean strain rate tensor. +, $x = -4.5$; ▽, $x = 0$; ○, $x = 5.2$; ●, $x = 10$; ◇, $x = 16$; △, $x = 20$; ×, $x = 27.1$. Internal layer is found at the last three stations.

and abruptly changes to $+45^\circ$ near the channel centreline. From the diffuser throat downstream, there is a settling region at $0 < x < 10$, within which the angle ϕ_1 exhibits significant variations. At the last three stations, the principal axis remains in nearly the same direction. It merely changes from -45° near the upper wall to -50° at $y = 0.1$. Thus, there exists a large region of the flow in which the principal axis of the rate of deformation tensor remains nearly unchanged. Turbulent eddies will thus be stretched along the nearly fixed direction as they are convected downstream. We

found from our visualization study that such a stretching process in the Obi diffuser is similar to, but less dramatic than, the process described by Wu & Durbin (2001).

In the flow over a bump (Webster *et al.* 1996), prior to the sudden change of C_{pw} near the trailing edge, the level of u'_{rms} is elevated and its peak displaced away from the wall to the central region of the boundary layer. As the streamwise pressure gradient changes from adverse to favourable, an inner peak of u'_{rms} appears while the outer peak owing to upstream adverse pressure gradient diminishes rapidly under the effect of the newly imposed favourable pressure gradient so that the wall-normal profiles of u'_{rms} show knee points, i.e. sharp turning, at the edge of internal layer. Sudden application of strong adverse pressure gradient at the throat of the Obi diffuser significantly elevates $\overline{u}'_{rms}$ near the upper flat wall, the local peak value at the throat is nearly 100% larger than the inlet peak. However, this elevated peak decays rapidly back to the original inlet peak level by $x = 10$ as a result of the levelling off of C_{pw} shown in figure 3. This process of rise and decay corresponds to the precipitous drop and subsequent stabilization in C_f discussed in figure 7. Under the effect of adverse pressure gradient, the elevated $\overline{u}'_{rms}$ in the region away form the wall bifurcates away from the inner peak and forms an outer peak. This outer peak is the one commonly observed when the boundary layer responds to an adverse pressure gradient. It shifts away from the wall with increasing streamwise distance from $x = 6.4$ to 14.4. This process can be discerned from figure 10. Because the flow is still under the influence of a weak adverse pressure gradient downstream of $x = 10$ the outer peak does not decay as quickly as in Baskaran *et al.* and Webster *et al.* Thus, in the Obi diffuser, internal layer signatures may also include a valley bottom at $y \approx 1.8$ separating the inner and outer peaks. The streamwise range within which such a signature is distinct is from $x = 15$ to 40, consistent with figure 6. Comparison of the computed turbulence intensity with experimental data at stations for $x > 40$ is less satisfactory, which is very similar to findings from Kaltenbach *et al.* (1999) and the other computational studies of the Obi diffuser. Kaltenbach *et al.* commented that the data of Obi *et al.* (1993) downstream of $x = 40$ are only of qualitative value for validation because of a possible scaling problem. No inflectional points can be found in the Reynolds shear stress and wall-normal intensity profiles. In wall-bounded shear flows, streamwise fluctuations respond to mean shear more quickly than Reynolds shear stress and wall-normal fluctuations, this has also been observed in laminar to turbulent transitional boundary-layer studies (see Wu *et al.* 1999). Antonia & Luxton (1971) reported that the growth of the internal layer thickness is proportional to $x^{0.79}$. Webster *et al.* (1996) found that their internal layer downstream of the bump trailing edge grew rapidly away from the wall and merged with the outer flow. The present internal layer itself is visualized in figure 16 using contours of r.m.s. streamwise turbulence intensity. An imaginary nearly horizontal line connecting the marked local tips of the contours close to the top wall can be considered approximately as the outer edge of the internal layer. It is obvious that the present internal layer exhibits negligible growth in the range of $16 < x < 40$.

We are interested in comparing the spectrum of $\overline{u}'$ at different streamwise stations as the flow experiences quasi-step change in streamwise pressure gradient near the throat and gradual relaxation further downstream. Figure 17 plots frequency spectrum $\phi(\omega)$ for $\overline{u}'$ as a function of ω near the outer edge of the internal layer at $x = -3$, 5.18, 10, 16, 20 and 30. No normalization was performed on the spectrum results. Grid spacing limits the highest frequency that can be locally resolved in the simulation, and this represents an implicit filter that is imposed by the grid on the flow field. The estimated Nyquist critical frequency ω_c based on the streamwise grid spacing and local value of $\langle\overline{u}\rangle$ is 570 at $x = -3$ and 230 at $x = 5.18$. Spectrum results at higher frequencies may

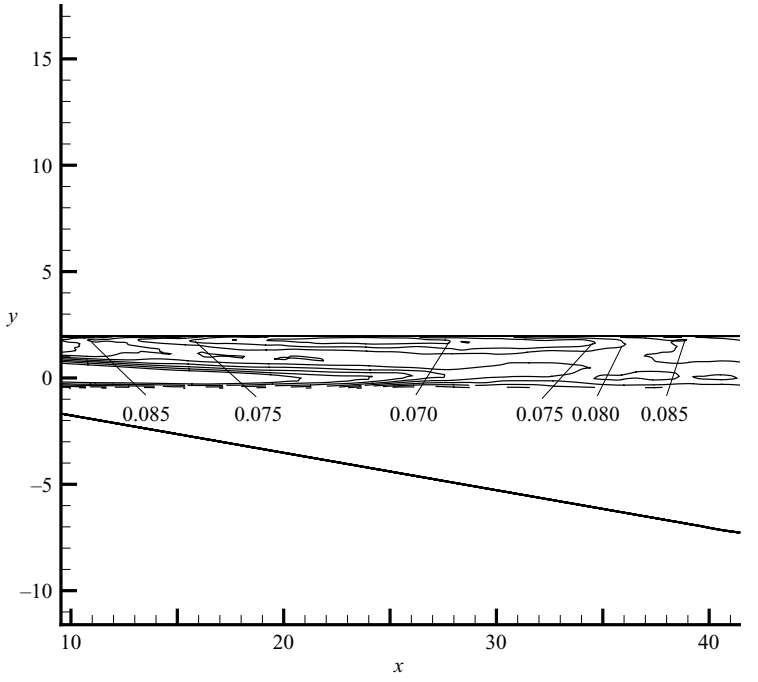

FIGURE 16. Visualization of the internal layer using contours of r.m.s. streamwise turbulence intensity.

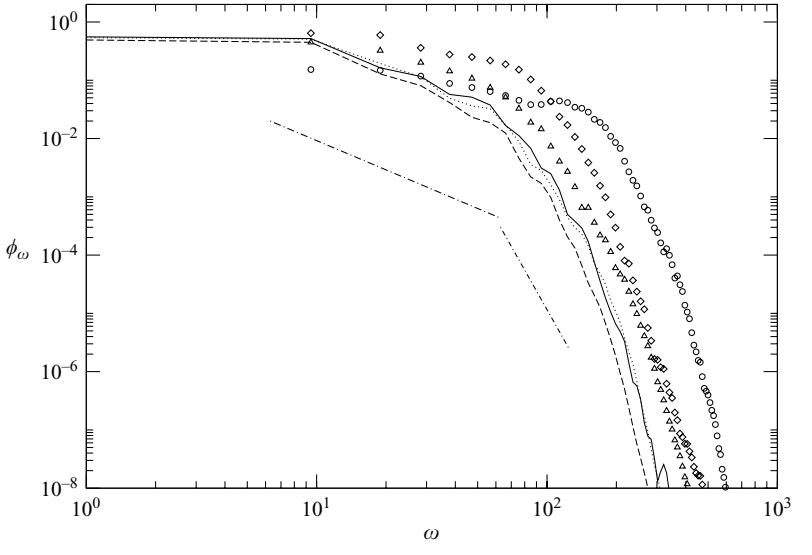

FIGURE 17. Frequency spectrum ϕ_ω for $\overline{u}'$ as a function of ω. ○, $x=-3$; ◇, $x=5.18$; △, $x=10$; solid line, $x=16$; dotted line, $x=20$; dashed line, $x=30$; for all the stations $y=1.8$ and $z=1.0$. The left and right chain-dotted lines represent the $-5/3$ and -7 slopes, respectively.

therefore be ignored on the figure. Compared to the profile at $x=-3$, $\phi(\omega)$ at 5.18 displays higher levels of low-frequency content and lower levels of high-frequency content. This clearly demonstrates that strong adverse pressure gradient enhances large-scale motions in the turbulent diffuser flow. From $x=5.18$ to $x=10$ there is a

further reduction in the energy level of high-frequency motions as the adverse pressure gradient remains strong in this region, see figure 3. The last three stations are in a region where the internal layer has formed as the adverse pressure gradient becomes rather weak and the skin friction has stabilized into a plateau. The spectra of $\overline{u}'$ at these locations ($x = 16$, 20 and 30) display decent collapse, suggesting that there is small streamwise variation in $\overline{u}'$ near the wall after initiation of the internal layer.

8. Concluding remarks

Azad & Kassab (1989) said in their concluding remarks that, 'it may also be conjectured that there is a new growth of a layer in the diffuser wall underneath the retarded, fully developed flow coming from the pipe into the diffuser.' Our results near the upper wall region of the asymmetric planar Obi diffuser support their conjecture, albeit at a much lower Reynolds number and also with qualifications.

The new layer is identified as an internal layer, but with slow growth. The mean streamwise velocity possesses a well-defined logarithmic slope inside the internal layer upto 80 wall units, and varies linearly with wall-normal distance outside the internal layer. One of the statistical indicators of an internal layer is an inflectional characteristic in the wall-normal profile of streamwise turbulence intensity. This may take the concrete form of a knee-point as reported in the external flow over a hill (Baskaran *et al.* 1987), or a valley as found in the present internal flow through a planar diffuser. Internal layers have a tendency to emerge in the relaxation zone downstream of a sudden change in streamwise pressure gradient. Examples of such abrupt changes in pressure gradient include the adverse to favourable drop at the trailing edge of the bump of Webster *et al.* (1996), as well as the favourable to adverse jump at the throat regions of the Azad diffuser (Okwuobi & Azad 1973), and the Obi diffuser. Obviously, one prerequisite for internal layer formation is that the abrupt change in pressure gradient may not lead to flow separation, though instantaneous flow reversal is not precluded. We argue that it is possible to relate the occurrence of an internal layer to the skin-friction coefficient C_f, which is directly related to the near-wall mean velocity gradient. For instance, a step increase in C_f is found after the trailing edge of the Webster bump corresponding to the adverse to favourable streamwise pressure gradient transition, followed by a gradual levelling off. Over the upper wall of the Obi diffuser, a rapid drop in C_f corresponding to the favourable to adverse pressure gradient jump is followed by a levelling off downstream of $x = 15$. The establishment and stabilization of a new level of C_f signals the birth of an internal layer and may be considered as an indicator.

Certain structural features of the internal layer were revealed by analysing large-eddy simulation results. It is found that the application of a strong adverse pressure gradient at the diffuser throat region enhances the low-frequency content of streamwise turbulent fluctuations. At various streamwise stations inside the internal layer, the power spectra with the same wall-normal coordinate nearly collapse. The correlation map of $R_{12}(x, y, z-z' = 0, t-t' = 0, x' = x, y')$ displays a distinctly different behaviour in the internal layer from that in the outer region. At the edge of the internal layer, a neck is formed in the correlation map. At zero time delay, streamwise fluctuations inside the internal layer at an upstream station have a relatively high degree of correlation with streamwise fluctuations in the outer region at a downstream station. Optimal time delay corresponds to eddies convected horizontally at the local mean streamwise velocity. At long time delays, near-wall streamwise fluctuations at the downstream station are more strongly correlated with upstream streamwise

fluctuations away from the wall. Visualization results in the Obi diffuser suggest the existence of organized vortices outside the internal layer. Galilean decomposition of instantaneous velocity vectors reveals a string of well-defined spanwise vortices which are convected downstream.

To some approximation, the present internal layer and the outer flow associated with it together constitute a distant analogue to the fundamental C-type of Couette–Poiseuille turbulent flows studied by Nakabayashi *et al.* (2004). They share broadly similar characteristics of mean and second-order turbulence statistics, but the total shear stress profiles are distinctly different. The role of the lower moving wall in the C-type flow is substituted by the high-speed fluid in the central region of the diffuser where the mean velocity $\langle\overline{u}\rangle$ varies linearly with the wall-normal coordinate. In this sense, the linearly varying high-speed flow in the outer region provides the necessary mean flow inflection mechanism for the fluid close to the wall, and may be regarded as one of the driving components in the present internal layer process. The location at which the total shear stress gradient changes sign serves as one the markers for the edge of the internal layer.

Finally, clarification should be added with reference to the discussion of Townsend (1976) that sudden changes in external conditions in boundary layers may result in an internal boundary layer that spreads from the section of change, and the layer outside the internal layer develops in almost the same way as in the original flow. The results from this study and from Wu & Squires (1998) suggest that internal layers may emerge in the relaxation zone downstream of a sudden change in streamwise pressure gradient. Furthermore, the layer outside the internal layer does not behave as if it were unperturbed, i.e. in the same way as in the original flow. On the contrary, the flow outside the internal layer displays distinct relaxation characteristics consistent with the removal of the strong pressure gradient. Admittedly, such observations are limited to the internal layers arising from sudden changes in streamwise pressure gradient. Other perturbation mechanisms, e.g. change in surface roughness, probably will result in an internal layer process not entirely the same as described in this paper.

Discussions with Juan Alonso, Sourabh Apte, George Constantinescu, Massimiliano Fatica, Sangho Kim, Krishnan Mahesh and Cliff Wall are acknowledged. We thank Peter Bradshaw for revising an earlier draft of the manuscript. This work is supported by the Advanced Simulation and Computing (ASC) program of the United States Department of Energy. The simulations were performed on the IBM terascale parallel machines at San Diego Supercomputing Center and at Lawrence Livermore National Laboratory.

REFERENCES

Adrian, R. J., Christensen, K. T. & Liu, Z. C. 2000 Analysis and interpretation of instantaneous turbulent velocity fields. *Exps. Fluids* **29**, 275–290.

Antonia, R. A. & Luxton, R. E. 1971 The response of a turbulent boundary layer to a step change in surface roughness. Part 1. Smooth to rough. *J. Fluid Mech.* **48**, 721–761.

Azad, R. S. 1996 Turbulent flow in a conical diffuser: a review. *Expl Therm. Fluid Sci.* **13**, 318–337. Special issue for Peter Bradshaw's 60th birthday.

Azad, R. S. & Kassab, S. Z. 1989 Turbulent flow in a conical diffuser: overview and implications. *Phys. Fluids* A **1**, 564–573.

Baskaran, V., Smits, A. J. & Joubert, P. N. 1987 A turbulent flow over a curved hill. Part 1. Growth of an internal boundary layer. *J. Fluid Mech.* **182**, 47–83.

Bradshaw, P. & Galea, P. V. 1967 Step-induced separation of a turbulent boundary layer in incompressible flow. *J. Fluid Mech.* **27**, 111–130.

Buice, C. U. & Eaton, J. K. 1997 Experimental investigation of flow through an asymmetric plane diffuser. PhD thesis, Department of Mechanical Engineering, Stanford University.

Choi, H. & Moin, P. 1990 On the space–time characteristics of wall-pressure fluctuations. *Phys. Fluids* **2**, 1450–1460.

Durbin, P. A. 1995 Separated flow computations with the $k-\epsilon-v^2$ model. *AIAA J.* **33**, 659–664.

Germano, M., Piomelli, U., Moin, P. & Cabot, W. H. 1991 A dynamic subgrid-scale eddy viscosity model. *Phys. Fluids* A **3**, 1760–1765.

Gravemeier, V. 2005 Variational multiscale large eddy simulation of turbulent flow in a diffuser. *Annual Research Briefs 2005*, pp. 257–268. Center for Turbulence Research, NASA Ames/Stanford University.

Iaccarino, G. 2001 Prediction of a turbulent separated flow using commercial CFD codes. *J. Fluids Engng* **123**, 819–828.

Kaltenbach, H. J., Fatica, M., Mittal, R., Lund, T. S. & Moin, P. 1999 Study of flow in a planar asymmetric diffuser using large eddy simulation. *J. Fluid Mech.* **390**, 151–185.

Keating, A., Piomelli, U., Balaras, E. & Kaltenbach, H. J. 2004 A priori and a posteriori tests of inflow conditions for large-eddy simulation. *Phys. Fluids* **16**, 4696–4712.

Kim, D. & Choi, H. 2000 A second-order time-accurate finite volume method for unsteady incompressible flow on hybrid unstructured grids. *J. Comput. Phys.* **162**, 411–428.

Lim, S. & Choi, H. 2004 Optimal shape design of a two-dimensional asymmetric diffuser in turbulent flow. *AIAA J.* **42**, 1154–1169.

Lindgren, B., Tornblom, O. & Johansson, A. V. 2002 Flow facility design and experimental studies of wall-bounded turbulent shear flows. PhD thesis, Royal Institute of Technology, Stockholm, Sweden.

Mahesh, K., Constantinescu, G. & Moin, P. 2004 A numerical method for large eddy simulation in complex geometries. *J. Comput. Phys.* **197**, 215–240.

Moser, R. D., Kim, J. & Mansour, N. N. 1999 DNS of turbulent channel flow up to $Re_\tau = 590$. *Phys. Fluids* **11**, 943–945.

Na, Y. & Moin, P. 1998 Direct numerical simulation of a separated turbulent boundary layer. *J. Fluid Mech.* **370**, 175–202.

Nakabayashi, K., Kitoh, O. & Katoh, Y. 2004 Similarity laws of velocity profiles and turbulence characteristics of Couette–Poiseuille turbulent flows. *J. Fluid Mech.* **507**, 43–69.

Obi, S., Aoki, K. & Masuda, S. 1993 Experimental and computational study of turbulent separating flow in an asymmetric plane diffuser. *Ninth Symp. Turbulent Shear Flows, Kyoto, Japan, August 16–19*.

Okwuobi, P. A. C. & Azad, R. S. 1973 Turbulence in a conical diffuser with fully developed flow at entry. *J. Fluid Mech.* **57**, 603–622.

Pierce, C. D. & Moin, P. 2004 Progress variable approach for large-eddy simulation of non-premixed turbulent combustion. *J. Fluid Mech.* **504**, 73–97.

Schlüter, J., Pitsch, H. & Moin, P. 2004 Large eddy simulation inflow conditions for coupling with Reynolds-averaged flow solvers. *AIAA J.* **42**, 478–484.

Skote, M. & Henningson, D. S. 2002 Direct numerical simulation of a separated turbulent boundary layer. *J. Fluid Mech.* **471**, 107–136.

Townsend, A. A. 1961 Equilibrium layers and wall turbulence. *J. Fluid Mech.* **11**, 97–120.

Townsend, A. A. 1965 Self-preserving flow inside a turbulent boundary layer. *J. Fluid Mech.* **22**, 773–797.

Townsend, A. A. 1976 *The Structure of Turbulent Shear Flow*, 2nd edn. Cambridge University Press.

Trupp, A. C., Azad, R. S. & Kassab, S. Z. 1986 Near wall velocity distributions within a straight conical diffuser. *Exps Fluids* **4**, 319–331.

Webster, D., DeGraaff, D. & Eaton, J. K. 1996 Turbulence characteristics of a boundary layer over a two-dimensional bump. *J. Fluid Mech.* **320**, 53–69.

Wu, X. & Durbin, P. A. 2001 Evidence of longitudinal vortices evolved from distorted wakes in a turbine passage. *J. Fluid Mech.* **446**, 199–228.

Wu, X., Jacobs, R., Hunt, J. C. R. & Durbin, P. A. 1999 Simulation of boundary layer transition induced by periodically passing wakes. *J. Fluid Mech.* **398**, 109–153.

Wu, X. & Squires, K. D. 1998 Numerical investigation of the turbulent boundary layer over a bump. *J. Fluid Mech.* **362**, 229–271.